A comparison of methods for determining watertightness test parameters of building façades

José M. Pérez-Bella[a], Javier Domínguez-Hernández[a,*], Enrique Cano-Suñén[a], Juan J. del Coz-Díaz[b], Francisco J. Suárez-Domínguez[b]

[a] *Department of Construction Engineering, Engineering and Architecture School, University of Zaragoza, María de Luna, s/n, 50018 Zaragoza, Spain.*

[b] *Department of Construction Engineering, University of Oviedo, Edificio Departamental Viesques nº 7, 33204 Gijón, Spain.*

Abstract

Watertightness tests allow evaluating the performance of building façades using standardised parameters that simulate real weather conditions, i.e., a combination of wind-driven rain and driving rain wind pressure. It has been a challenge for researchers to experimentally test simultaneous wind and rain conditions in a rigorous manner. However, two new methods have minimised this problem, creating a precise relationship between the experimental result and the expected performance of the façade under real conditions and vice-versa. This article reviews both alternative methods and analyses their theoretical foundations and comparative advantages. In addition, the two methods are applied in the same case study, analysing the exposure conditions for a generic façade located in Bilbao (Spain). Ten-minute climatic records gathered over 14 years at the city airport have been used for this analysis. The comparative results show an adequate convergence between both procedures. However, their methodological differences would suggest using each one for different specific applications.

Keywords

Watertightness; Test parameters; Climate loads; Bayesian probability; Pareto front; Façades

[*] Corresponding author. Department of Construction Engineering, University of Zaragoza (UZ), María de Luna, s/n, 50018, Zaragoza, Spain. Tel.Fax: +34 976 76 21 00.
E-mail address: javdom@unizar.es (Javier Domínguez-Hernández)

1. Introduction

Limiting the penetration of atmospheric water in building façades is a key task for preventing illnesses [1-2], increasing energy efficiency [3-4] and reducing building maintenance costs [5-8]. Currently, each normative framework uses different watertightness tests to assess the resistance of façade designs against this penetration [9-14]. In these tests, this resistance is related to the ability of the sample façade to withstand a constant supply of water (water spray rate) and a specific pressure difference (ΔP) between their outer and inner surfaces, thereby preventing the passage of liquid water into its inner surface. However, there are significant differences among water spray rate values, ΔP, and duration of the exposure interval used in these tests [15].

Moreover, until recently, there have been no completely satisfactory procedures for estimating the value of parameters that recreate the real exposures under operating conditions [15-19]. However, two methods have recently been developed to accurately determine the parameter values that should be used to verify a particular watertightness performance in building façades [19-22]. Thus, for the first time, both methods allow assessing the occurrence probability of simultaneous rainfall and wind velocity events (i.e., the expected performance of the facada under a specific operation condition or equivalent test parameters).

To this end, the methods start from different theoretical foundations, resulting in two independent procedures to resolve the same problem. This article reviews the characteristics of these methods and analyses their possibilities and uncertainties. The analysis is performed by applying both methods to the same case study, a generic façade from the city of Bilbao (Spain). A comparison of the obtained results can be used to analyse the convergence of both procedures.

Together, this study offers a broad perspective of the two most complete methods for relating the real exposure conditions to water penetration with the test parameters used to determine the performance of façade designs. The results shown suggest that the application of either method would contribute to improving current façade designs in any location and under any operating condition. However, each

method has specific characteristics that would make it recommendable for use in different concrete applications.

2. Background

In watertightness tests, full-scale façade models are subjected to a constant water spray rate and increasing ΔP rate over short exposure intervals. The maximum ΔP that the design withstands without allowing water to pass to the interior face of the model characterises its watertightness. The water spray rate and ΔP are attempts to simulate the two most influential climatic conditions in the water penetration of façades: wind-driven rain (WDR) and driving rain wind pressure (DRWP).

The water spray rate varies for each test, normally between 2 and 4 l/m^2min. In any case, a continuous flow of runoff water over the model surface must be ensured. Meanwhile, the applied ΔP acts as the main test parameter, increasing by intervals until watertightness is lost. The ΔP ranges used also vary for each test, as well as the exposure time interval of these ranges [9-14].

However, these standardised parameters do not adequately represent façade exposure under all possible operating conditions. WDR and DRWP exposures vary by storm event and location and depend on the rainfall intensity and concurrent wind velocity [23-26]. Other aspects, such as the building geometry, height or surrounding terrain, also influence the quantity of water and wind pressure received by each point of the building enclosure [27-30].

The influence of both climatic conditions on water penetration also depends on the surface finish of the façade [17, 31]. On new façades, without pores or major defects (openings < 1 mm), only a high DRWP exposure is able to produce water penetration, and WDR becomes a secondary factor. At a practical level, watertightness tests only simulate high ΔP and low water spray rate. Given that the façade samples are

created for the test and lack major surface defects, the ΔP parameter is always used as the main test parameter (maximising applied pressure), and the water spray rate falls to secondary importance.

To establish more realistic watertightness tests, the least favourable WDR (i.e., water spray rate) and DRWP (i.e., ΔP) which may occur on each façade should be simulated. For this purpose, one can set the frequency or return period associated with the climatic conditions that the façade should withstand without losing watertightness. Taking into consideration longer return periods to evaluate watertightness performance leads to simulating more infrequent and extreme WDR and DRWP exposures (i.e., more demanding test parameters). Thus, the return period for climatic conditions to be examined (normally 10-30 years) [15, 32] can be used as a design factor that defines the operating performance of the building façade.

Calculating WDR and DRWP exposure combinations associated with a specific return period has represented a challenge for researchers [15-18] that has finally been resolved using both alternative methods [19-22]. A presentation and analysis of the theoretical foundations, comparative advantages and differences of each method are given below.

2.1 Pareto-front analysis

This method allows estimating extreme combinations of wind velocity and rain intensity for different locations and return periods. For this purpose, only the highest climatic records were selected using the notion of Pareto efficiency. These records are then subjected to a Point-Over-Threshold (POT) analysis [33-36]. Each estimated extreme combination for a set return period allows obtaining the WDR and DRWP values that define the test parameters to be used (water spray rate and ΔP, respectively) [22].

To apply the method, available climatic records of the location should be represented using a scatterplot (X: wind velocity U; Y: rainfall intensity R_h). These records should match with short time intervals, similar in duration to those of the tests (5-20 min). The farthest points from the origin represent the most

extreme records. Thus, the Pareto efficiency criterion can be used to determine the Pareto-optimal front that connects each Pareto-point (i.e., those records for which there is no higher value in either the X or Y axis, without simultaneously leading to a lower value in the other axis). The records contained in this first Pareto-front represent the R_h and U values that have caused the highest combinations of WDR and DRWP exposures over the data collection period. Discarding the points of this first Pareto-front, a second Pareto-front between the remaining records can be identified, and the first 10 Pareto-fronts can similarly be determined.

The Pareto-points contained in the first 10 Pareto-fronts represent a sufficiently low number of records above a high exposure threshold. Thus, proposing a POT analysis to determine R_h-U combinations associated with different return periods is reasonable. However, to apply the POT analysis, each Pareto-point defined by two variables (R_h-U) should be previously associated with a single representative value.

For this, the 10 straight lines that best fit the records of the first 10 Pareto-fronts should be determined. The mean slope of these lines can be calculated to determine the intersection between the mean slope line that passes through each Pareto-point and one of the axes (X or Y). Thus, each Pareto-point is associated with a unique intersection value that can be used in the POT analysis. To apply this analysis, a Generalised Pareto Distribution (GPD) is defined that is fitted to the cumulative distribution function (CDF) of the intersection values, thereby allowing the intersection associated with a specific return period to be estimated.

Fixing a return period to assess the façade's watertightness performance, the mean slope line based on the estimated intersection value represents the R_h-U combinations associated with that return period in the location (i.e., it represents approximately the Pareto-front associated with this return period).

To limit maximum U and minimum R_h combinations, only the Pareto-point of highest U of each of the first 10 Pareto-fronts are selected, determining a line of best fit. Similarly, selecting only the Pareto-point of the greatest R_h of each front can also define a best fit line that limits the combinations of maximum R_h

and minimum U. The intersection points between these two limit lines and the mean slope line represent the extreme R_h-U combinations that may arise in the enclosure for the set return period. The bisecting line of both limit lines can also be used to define average combinations of both climatic records [22]. Fig. 1 shows a schematic summary of these steps. An application example of the method is also developed in section 3.1.

The parameters for the water spray rate (i.e., WDR) and ΔP (i.e., DRWP) can be estimated based on these extreme R_h-U values via different semi-empirical approximations [17, 27, 37-40], CFD [28-30, 41-43] or combinations thereof [21]. The operating condition of each façade should be considered when making these approximations (e.g., the height or roughness of the surrounding terrain) as this condition influences the WDR and DRWP values. Thus, when a pair of extreme R_h-U values associated to a fixed return period is determined, the test parameters will vary for each possible operating condition of the façade.

Fig. 1. Overall scheme of Pareto-front method and its graphic procedure.

2.2 Bayesian performance-based analysis.

This second method enables the estimation of the simultaneous WDR and DRWP values associated with a specific return period. For this purpose, the return period associated with any combination of WDR and DRWP exposure is estimated via a Bayesian analysis of conditioned probability [19]. To resolve this probability equation, the WDR and DRWP values are estimated using approximations similar to those of the previous method. Thus, the same prior climactic records are used in this method. The solution to the resulting system of equations allows the determination of the test parameters associated with specific design performances, operating conditions and locations.

To estimate the $DRWP_z$ (Pa) value, the Bernoulli equation can be used (Eq. 1), considering the height z (m) of the façade and the roughness of the surrounding terrain α (-) by means of the wind profile power-law [44]. The records for wind velocity U_{10} (m/s) are only those that are simultaneous with precipitation and are taken under reference conditions (open and clear areas at a height of 10 m above ground level) [45]. For a conservative estimate, a pressure coefficient C_p of 1 and a constant air density ρ of 1.2 kg/m^3 can be used [46].

$$DRWP_z = C_p \cdot \frac{1}{2} \cdot \rho \cdot \left(U_{10}\right)^2 \cdot \left(\frac{z}{10}\right)^{2\alpha} \tag{1}$$

To estimate WDR exposure, one can combine the semi-empirical equation defined by Straube and Burnett [27], the terminal velocity value for raindrops determined by Dingle and Lee [47] and the calculation for the predominant diameter of water droplets developed by Cornick et al. [48]. As a result, Eq. 2 represents the WDR_z value (l/m^2) at the uppermost corners of a building of height z (m) and surroundings α (-), where R_h (l/m^2) represents the intensity of precipitation and U_{10} (m/s) the simultaneous records of wind velocity.

$$WDR_z = \frac{U_{10} \cdot \left(\frac{z}{10}\right)^{\alpha}}{-0.184478 \cdot \left(R_h\right)^{-1} + 5.471534 \cdot \left(R_h\right)^{-0.768} - 0.988909 \cdot \left(R_h\right)^{-0.536} + 0.061193 \cdot \left(R_h\right)^{-0.304}} \tag{2}$$

Finally, the combined probability of two values for $WDR_{z\,i}$ and $DRWP_{z\,i}$ (i.e., its combined return period) can be established as a conditional probability analysis using Bayes' Theorem (Eq. 3) [49].

$$\frac{1}{Return\ period} = P\left(WDR_{z\,i} \cap DRWP_{z\,i}\right) = P\left(DRWP_{Z\,i}\right) \cdot P\left(WDR_{z\,i} \mid DRWP_{z\,i}\right) \tag{3}$$

Given that $DRWP_{z\,i}$ depends only on the climatic variable U_{10} (see Eq. 1), its probability may be substituted by the occurance probability of the necessary $U_{10\,i}$ value. Similarly, the probability of $WDR_{z\,i}$ if there is a simultaneous wind velocity $U_{10\,i}$ (see Eq. 2) may be substituted by the occurance probability

of the necessary $R_{h\,i}$ value (Eq. 4). To calculate both probabilities P($U_{10\,i}$) and P($R_{h\,i}$), this method suggests an analysis of the annual maxima series of the two climatic records and the application of the Gumbel Distribution [50].

$$\frac{1}{Return\ period} = P\left(WDR_{z\,i} \cap DRWP_{z\,i}\right) = P\left(U_{10\,i}\right) \cdot P\left(R_{h\,i}\right) \tag{4}$$

The resulting three-equation system (Eqs. 1, 2, 4) raises five unknowns (WDR_z, $DRWP_z$, *Return period*, R_h and U_{10}) for each façade defined by its operating conditions z and α. By setting two of these unknowns, the remaining three can be determined. Thus, setting the WDR_z as equal to the water spray rate used in the test and determining a *Return period* for evaluating the watertightness design performance yields the $DRWP_z$ (i.e., ΔP) value that must be overcome in the test. Similarly, by setting the water spray rates and ΔP surpassed during a test (WDR_z and $DRWP_z$, respectively*)*, the design *Return period* of the façade for any operating condition *z*-α in the location can be obtained. Fig. 2 shows a schematic summary of the steps described here. An application example of the method is also developed in section 3.2.

Given that ΔP is always the main test parameter for watertightness tests, setting the $DRWP_z$ value and the design *Return period* to calculate the WDR_z (i.e., the water spray rate) to surpass does not make practical sense [19]. Similarly, although the equation system always leads to a dual solution (higher U_{10} - lower R_h; higher R_h – lower U_{10}), only the first solution ends up being interesting for application to these tests as it offers a greater value for DRWP (i.e., ΔP).

A later development of this method has also defined an additional step for extrapolating those results to different exposure intervals using only the original climatic records [20]. Thus, the necessary test parameters to recreate different exposure intervals from those of the original records can be estimated. In turn, this allows for a comparison of the results obtained from watertightness tests with different exposure intervals.

Fig. 2. Overall scheme of the Bayesian performance-based method and its equation system solution.

2.3 Discussion

The different theoretical approximations used by both procedures and its development establish the uncertainties and comparative advantages between them. Thus, different methodological aspects in the Pareto-front analysis that may affect the accuracy and usefulness of the estimated test parameters can be highlighted:

- Frequently, several Pareto-points of a Pareto-front are due to the same storm event and would thus be associated with a single return period. Identifying and discarding those points generated by events that are already included in prior Pareto-fronts is a complex task, and the criteria adopted for this elimination can alter the geometry of the fronts and thus the final results. The number of Pareto-fronts analysed (10 in the description shown herein) is also an arbitrary factor. These characteristics can alter the slope of the best fit lines and, thus, the mean slope used for the POT analysis. The simplification of the Pareto-fronts using best fit lines is another source of uncertainty as these fits are not precise [22]. Additionally, the mean slope used can be determined based on one fit line determined from all Pareto-points of the first 10 Pareto-fronts.
- For each operating condition and return period, the method determines a unique combination of test parameters (water spray rate and ΔP). Modifying both test parameters to evaluate each possible operating condition of the façade is not a functional proposition. In turn, using the method to establish water spray rate and ΔP standardised ranges for the tests would reduce the ability of the test to precisely estimate watertightness performance under each specific service condition.

- The calculation is also difficult to automate due to the high number of intermediate steps and laborious analysis that they require (spreadsheet programs and tools for extreme value analysis are needed). However, the results found only refer to a single exposure interval (equal to the duration of the R_h–U records). Defining and adding additional steps would be necessary to estimate the test parameters associated with different exposure intervals used in the current tests.
- Although the three extreme combinations obtained can be interesting at the theoretical level, only the result for the extreme U combination is of interest for practical application in watertightness tests. The other combinations (extreme R_h and moderate R_h-U) determine lower DRWP values and thus a lower main test parameter ΔP.

Nevertheless, the method directly analyses recorded physical phenomena, leading to an exhaustive analysis of simultaneous R_h and U conditions (and with them, of WDR and DRWP exposures) on the façades of the location, which is a positive outcome. The limits of the extreme combinations identified can also be used to improve the standardised ranges for current test parameters.

The Bayesian performance-based analysis also shows methodological aspects that affect the precision and usefulness of its results:

- The mathematical approximations adopted to define Eqs. 1 and 2 (e.g., the wind profile power-law, terminal velocity of raindrops, or diameter of water droplets) can change the precision of the results. There are other equations that can also be used [15, 21], which would result in different test parameters. In addition, the method does not directly analyse the statistical simultaneity of the R_h-U_{10} records but instead uses these approximations to define their conditioned probability. Thus, an additional source of uncertainty is added to the results.
- In turn, the equation system may not produce a result in certain cases, if the curves of both equations do not intersect (see Fig. 2). These cases can occur under conditions of high WDR exposure and relatively short return periods (which translate into lower DRWP values). However, this situation is

not simulated in the tests in which the water spray rate is always reduced and comparatively lower than the main test parameter ΔP.

- The use of the Gumbel Distribution (based on annual maxima series) for calculating the occurrence probability of $R_{h\,i}$ and $U_{10\,i}$ values is less reliable than the POT analysis for limited historical records [51]. The calculation of the combined probability of $WDR_{z\,i}$ and $DRWP_{z\,i}$ exposures also does not guarantee that both values will occur during the same storm event.
- Finally, the method does not identify the most unfavourable WDR and DRWP combinations that can arise on a façade for the set return period. Instead, it determines the most unfavourable R_h and U_{10} combinations (i.e., $DRWP_z$ or ΔP) that may arise for the set return period and a WDR exposure equal to the water spray rate standardised in the test.

However, the Bayesian method allows for a functional and automatable application, making large-scale applications possible through specific tools [20]. If the set water spray rate for each test is known, the method is able to use the surpassed ΔP to determine the design return period under any operating condition in the location. Similarly, it can estimate the ΔP that should have been surpassed in the test to simulate a specific design return period. In addition, modifying current test equipment is not necessary because the method adapts to any exposure interval or water spray rate. All of these factors allow established parameters for different tests to be compared, assessing similar return periods and façade operating conditions [20]. Similarly, this method also enables one to take advantage of test results already performed on façade systems available on the market by estimating their performance under any operating condition and on any location.

3. Application of both methods to a case study in Bilbao (Spain)

Both methods are applied here to define test parameters associated with the same generic façade in Bilbao (Spain), which was 10 meters in height, located in flat surroundings, and free from obstacles. The

watertightness performance of the generic façade was set according to different return periods for climatic conditions for which the enclosure would maintain watertightness.

Bilbao is located on the northern coast of the Iberian Peninsula and is characterised by a high level of wind-driven rain exposure [52-53] and strong Atlantic winds occurring simultaneously with precipitation [53-54]. The meteorological station is located in the city airport and shares the open surroundings of the proposed façade. The availability of 10-minute climatic data, gathered over 14 years (1997-2010) by the Spanish Meteorological Agency (AEMET), determined the site selection. The number of gaps in the data is less than 7% (due to errors, meteorological instrument failures and maintenance works that cannot be associated with extreme weather conditions), giving a representative series of records to compare both methods.

3.1 Pareto front analysis

Following the procedure described above, Fig. 3 represents a scatterplot with the simultaneous combinations of wind velocity U_{10} (m/s) and precipitation intensity R_h (l/m^2 10 min) present in the available 10-minute records. The first 10 Pareto-fronts have been identified on this scatterplot, and for each one, the slope of the line that best adjusts to its Pareto-points has been obtained. These slopes allow for the calculation of the mean slope, representing the slope that a generic Pareto-front would have in light of these records. Drawing a straight line with this mean slope from each Pareto-point provides different intersections with the Y axis. In total, 174 Pareto-points were identified in these first 10 Pareto-fronts, for a total of 174 Y-intersections (for the sake of simplicity, Fig. 3 only shows the line of the highest Y-intersection).

Fig. 3. Scatterplot showing 15 years of 10-minute rainfall intensities and simultaneous wind velocities (*grey dots represent Pareto-points not contained in the first 10 Pareto-fronts).*

Given that these Y-intersections represent the least favourable events from all available records, a POT analysis can be used to estimate the probability (i.e., return period) associated with each possible intersection value. Fig. 4 shows the empirical CDF for the Y-intersections and the theoretical CDF created from the best fit GPD for the empirical distribution. The Method of Moments was used to adjust the parameters of this GPD, also verifying the Mean Squared Error between both distributions.

Fig. 4. Empirical CDF of intersection values (grey line) and theoretical CDF of a GPD with γ = 0.0161647, σ = 1.77267 and optimal threshold u = 10.1895 (black line).

The intersection values associated with different return periods can be obtained using Eq. 5, considering the time period analysed (n_{year} = 14) and the number of intersections above the optimal threshold (N_u = 81). Table 1 shows the estimated intersection points for different return periods and the mean slope lines that represent a generic Pareto-front associated with each one.

$$\text{Y-Intersection} \approx u + \frac{\sigma}{\gamma}\left[\left(\frac{n_{year}}{N_u \cdot \text{Return period}}\right)^{-\gamma} - 1\right] \quad (5)$$

Table 1. Intersection points and line equations associated with different return periods, obtained via POT analysis.

Fig. 5 shows these representative lines for different return periods and their intersection with the extreme-combination lines of most interest (dotted lines). Thus, the upper dotted line corresponds to the best fit line for the points of highest R_h in the first 10 Pareto-fronts, and the lower dotted line corresponds to the points of highest U_{10}. The intermediate dotted line (bisector of the previous two lines) can be used to estimate moderate combinations of both climatic variables.

Fig. 5. The line intersections represent the interesting climate variables for different exposure combinations and return periods *(maximum R_h or U_{10} Pareto-point of each Pareto-front are also shown)*.

Finally, Table 2 gathers the R_h and U_{10} intersection values between the lines shown as well as the WDR and DRWP exposures (i.e., water spray rate and ΔP) that should be applied in the watertightness tests to simulate each return period and extreme combination for the façade in question (z = 10 m). For a homogenous comparison of both procedures, the same approximations for estimating the WDR and DRWP exposures from the R_h and U_{10} values were used (Eqs. 1 and 2). Thus, the divergences that are truly attributable to each of the theoretical approaches can be estimated without alteration by these estimates.

Table 2. Watertightness test parameters calculated by the Pareto-front method for different return periods and exposure combinations in the considered façade (z = 10 m, Bilbao).

3.2 Bayesian performance-based analysis

Following the above procedure involves using the system composed of Eqs. 1, 2 and 4. An annual maxima series analysis based on the Gumbel Distribution is used to calculate the probabilities of Eq. 4. The result is Eq. 4', where the values for mode λ and dispersion parameter β for each climatic variable depend only on the annual maxima series recorded in the location. The detailed calculation of these Gumbel Distribution parameters λ and β for each variable is shown in Tables 3 and 4.

$$\frac{1}{\text{Return period}\left(WDR_{z\,i} \cap DRWP_{z\,\mathrm{i}}\right)} = \left(1-\exp^{-\exp^{-\left(U_{10\,\mathrm{i}}-\lambda(U_{10})\right)/\beta(U_{10})}}\right)\cdot\left(1-\exp^{-\exp^{-\left(R_{h\,\mathrm{i}}-\lambda(R_h)\right)/\beta(R_h)}}\right) \quad (4')$$

Table 3. Summary of the highest annual precipitation recorded in a 10-minute interval and the calculation of Gumbel distribution parameters.

Table 4. Summary of the highest annual wind velocity recorded in a 10-minute interval and the calculation of the Gumbel distribution parameters.

Normally, the water spray rate of the test and the design return period are considered to determine the ΔP value to surpass in the watertightness trial. However, to compare both methods, the system composed of Eqs. 1, 2 and 4' was solved by setting the return periods and WDR values that were already identified by the Pareto-front analysis for different extreme combinations (see Tables 2 and 5). The results DRWP (i.e, ΔP), R_h and U_{10} permit an analysis of divergences between both procedures for identical conditions.

As indicated in section 2.3, the equation system offers two possible solutions: a solution with a higher R_h value and another solution with a higher U_{10} value. An intermediate solution can also be defined,

considering the middle point between both previous solutions. For example, Fig. 6 shows the solutions associated with 5- and 10-year return periods for the extreme R_h combination. The return period was set as 5 and 10 years, and the WDR value was set as 20.72 and 26.78 l/m^2 10 min, respectively (see Table 2). From a practical standpoint, the most interesting solution for watertightness tests is the one with a higher U_{10} value as it will determine higher and more demanding DRWP values (i.e., ΔP) for testing.

Fig. 6. Graphic solution of the Eqs. 2 and 4' system for the extreme R_h combination (Table 2): 5-year return period (black lines) and 10-year return period (grey lines).

As shown, the system of equations proposed in the Bayesian method does not solve the extreme R_h combination for the WDR values presented in Table 2 and associated with return periods longer than 5 years. In these cases, the curves shown in Fig. 6 do not intersect, and thus a mathematical solution cannot be found. This lack of a solution means there is no DRWP value that can occur with the set WDR, within the determined return period. The necessary return period to produce the set WDR would itself be greater than that proposed in Table 2. Table 5 demonstrates this impossibility and the results for the other extreme combinations.

Table 5. Watertightness test parameters calculated by the Bayesian performance-based method for different return periods and exposure combinations in the considered façade (z = 10 m, Bilbao). *The values fixed for solving the equation system are shown in bold type.*

3.3 Comparison of results

Using the results shown in Tables 2 and 5, Fig. 7 compares the estimated DRWP values (i.e., ΔP) by each method for different return periods and the extreme U_{10} combination. This combination represents the least favourable conditions for watertightness tests as it returns the highest ΔP values for developing the test. These values show divergences of less than 15%, and are identical for a 30-year return period. For longer return periods, the Bayesian method returns slightly more conservative test parameters.

One may also observe how the climatic variables R_h and U_{10} estimated by both methods show differences of 10% and 8% respectively, for identical return periods and WDR values. Given that the approximations for the exposure to other altitude z conditions or α surroundings are based on these R_h and U_{10} variables (Eqs. 1 and 2), parameters estimated by both methods for any other operating condition will have a similar convergence.

Fig. 7. Estimated ΔP values calculated by both methods to simulate extreme U_{10} combinations for the same WDR values and return periods in the considered façade (z = 10 m, Bilbao).

If DRWP or ΔP values associated with the WDR exposures identified in the moderate R_h-U_{10} combination are compared, a small difference is also observable. Fig. 8 represents the estimated ΔP values for different return periods as well as the solutions of higher R_h and U_{10} necessary for calculating the moderate combination in the Bayesian method (see Fig. 6). The R_h and U_{10} values show differences of less than 7% and 6%, respectively, whereas the maximum divergence between DRWP (i.e., ΔP) values does not exceed 10%.

Again, the Bayesian method determines slightly more demanding test parameters than the Pareto-front analysis, remaining on the conservative side of any possible return period. As in the prior combination, these differences would be extrapolatable to any other operating condition in the location. In any case,

this moderate combination would impose less demanding values on the main test parameter (ΔP), which would suppose more favourable conditions for conducting the watertightness test.

Fig. 8. Estimated ΔP values calculated by both methods to simulate moderate U_{10}-R_h combinations for the same WDR values and return periods in the considered façade (z = 10 m, Bilbao).

For the extreme R_h combination, the absence of the solution to the Bayesian method equation system prevents the comparison of methods. As such, there is no mathematical value for DRWP or ΔP when combined with the WDR value presented in Table 5, which can arise during the specific return period. The interpretation (based on the Bayesian analysis) is that the WDR values identified by the Pareto-front analysis could not arise during these return periods and could only exist in longer return periods. However, this extreme combination does not represent the test scenarios, where the water spray rate fills a secondary role compared to the main test parameter ΔP.

4. Conclusions

This study is a comprehensive comparison of two alternative methods developed for determining realistic parameters to façade watertightness tests. Both methods are able to relate the real climatic conditions and the parameters used in these tests, based on a performance criterion. This should help to improve the current façade designs, accurately characterising its watertightness performance. By applying the Bayesian and Pareto-front methods to the same case study, the test parameters obtained are reasonably similar, with the Bayesian performance-based method being slightly more conservative. In order to completely validate the convergence of these methods would be advisable to extend the analysis to other

locations, climates and datasets. However, the results presented suggest an adequate overall convergence of both methods.

In addition, a theoretical comparison has identified the potential and uncertainties present in both methods, opening the door for future improvements. The Bayesian method is ideal for efficient use in the construction industry, given its greater functionality and potential of automation. So, the results of a standarised test can be used to assess the watertightness performance of a façade system under any operating condition. However, the need to use the water spray rate of the test to resolve the equation system may lead to omit the simulation of the most extreme climatic combinations. Therefore, the review of this test parameter, establishing more suitable and adjusted test values for reasonable return periods can improve the reliability and accuracy of the Bayesian method. In this regard, the Pareto-front analysis is capable of determining realistic extreme limits for these combinations and so it could be used to review the current standarised water spray rates in a general way (the practical application of this method for each operating condition is not functional).

Thus, both procedures can contribute to improve the current design of building façades: allowing a functional assessment of its watertightness performance in any operating condition or location (Bayesian method), and adjusting the current water spray rates for standardised tests (Pareto-front method), indirectly increasing the reliability and accuracy of the Bayesian method.

Acknowledgements

These results were obtained from data provided by the Spanish Meteorological Agency, Ministry of Environment, Rural and Marine Affairs (AEMET). This work was partially financed by the Spanish Ministry of Science and Innovation co-financed with FEDER funds under the Research Project BIA2012-31609.

References

[1] Haverinen-Shaughnessy U. Moisture as a source of indoor air contamination. In: Proceedings of the EnVIE Conference on Indoor Air Quality and Health for EU Policy. Helsinki: 2007.

[2] WHO. Environmental burden of disease associated with inadequate housing. Methods for quantifying health impacts of selected housing risks in the WHO European region. Copenhagen: World Health Organization; 2011.

[3] Sanders C. Heat, air and moisture transfer in insulated envelope parts: Environmental conditions. International Energy Agency, Annex 24, Final report, vol. 2. Leuven: 1996.

[4] Del Coz JJ, Rabanal FP, García PJ, Domínguez J, Rodríguez B, Pérez JM. Hygrothermal properties of lightweight concrete: Experiments and numerical fitting study. Constr Build Mater 2013; 40:543-55. (doi: 10.1016/j.conbuildmat.2012.11.045)

[5] Rousseau J. Rain penetration and moisture damage in residential construction. In: Building science insight'83, seminar on humidity, condensation and ventilation in houses. Canada: 1983.

[6] Waldum AM. Restoration of masonry facades, renders and final coats in a severe climate. Composition and durability of old rendering mortars described and suggestions made for the composition of coating system for old masonry walls in severe climate. Build Res Inf 1993; 21(1):51–55. (doi:10.1080/09613219308727255)

[7] Tang W, Davidson CI, Finger S, Vance K. Erosion of limestone building surfaces caused by wind-driven rain. 1. Field measurements. Atmos Environ 2004; 38(33): 5589-99. (doi:10.1016/j.atmosenv.2004.06.030)

[8] Kvande T, Lisø KR. Climate adapted design of masonry structures. Build Environ 2009; 44(12):2442-50. (doi:10.1016/j.buildenv.2009.04.007)

[9] EN 12155:2000. Curtain walling. Watertightness. Laboratory test under static pressure. European Committee for Standardization.

[10] EN 12865:2001. Hygrothermal performance of building components and building elements. Determination of the resistance of external wall systems to driving rain under pulsating air pressure. European Committee for Standardization.

[11] AAMA 501.1:2005. Standard test method for water penetration of exterior windows, curtain walls and doors using dynamic pressure. American Architectural Manufacturers Association.

[12] AS/NZS 4284:2008. Testing of building façades. Australian and New Zealand Standards Institution.

[13] ASTM E331-00:2009. Standard test method for water penetration of exterior windows, skylights, doors, and curtain walls by uniform static air pressure difference. American Society for Testing and Materials.

[14] ASTM E547-00:2009. Standard test method for water penetration of exterior windows, skylights, doors, and curtain walls by cyclic static air pressure difference. American Society for Testing and Materials.

[15] Sahal N, Lacasse MA. Proposed method for calculating water penetration test parameters of wall assemblies as applied to Istanbul, Turkey. Build Environ 2008; 43:1250–60. (doi:10.1016/j.buildenv.2007.03.009)

[16] Choi ECC. Criteria for water penetration testing. In R. Kudder J. & J. Erdly L. (Eds.), Water leakage through building facades (pp. 3–16), ASTM STP 1314. West Conshohocken, 1998.

[17] Cornick SM, Lacasse MA. A review of climate loads relevant to assessing the watertightness performance of walls, windows, and wall–window interfaces. Journal of ASTM International 2005; 2(10):1–16. (doi:10.1520/JAI12505)

[18] Cornick SM, Lacasse MA. An investigation of climate loads on building façades for selected locations in the US. Journal of ASTM International 2008; 6(2):1–17. (doi:10.1520/JAI101210)

[19] Pérez JM, Domínguez J, Rodríguez B, del Coz JJ, Cano E. A new method for determining the water tightness of building facades. Build Res Inf 2013; 41(4): 401–414. (doi:10.1080/09613218.2013.774936)

[20] Pérez JM, Domínguez J, Rodríguez B, del Coz JJ, Cano E, Navarro A. An extended method for comparing watertightness tests for facades. Build Res Inf 2013; 41(6): 706–721. (doi:10.1080/09613218.2013.823538)

[21] Van den Bossche N, Lacasse MA, Janssens A. A uniform methodology to establish test parameters for watertightness testing. Part I: A critical review. Build Environ 2013; 63:145–56). (doi:10.1016/j.buildenv.2012.12.003)

[22] Van den Bossche N, Lacasse MA, Janssens A. A uniform methodology to establish test parameters for watertightness testing. Part II: Pareto front analysis on co-occurring rain and wind. Build Environ 2013; 63:157–67). (doi:10.1016/j.buildenv.2012.12.019)

[23] Chand I, Bhargava PK. Estimation of driving rain index for India. Building Environ 2002; 37: 549-54. (doi:10.1016/S0360-1323(01)00057-9)

[24] Blocken B, Carmeliet, J. A review of wind-driven rain research in building science. J. Wind Eng Ind Aerodyn 2004; 92(13):1079-130. (doi:10.1016/j.jweia.2004.06.003)

[25] Giarma C, Aravantinos D. Estimation of building components' exposure to moisture in Greece based on wind, rainfall and other climatic data. J Wind Eng Ind Aerodyn 2011; 99: 91-102. (doi:10.1016/j.jweia.2010.12.001)

[26] Pérez JM, Domínguez J, Cano E, del Coz JJ, Alonso M. Global analysis of building façade exposure to water penetration in Chile. Build Environ 2013;70:284-297. (doi: 10.1016/j.buildenv.2013.09.001)

[27] Straube JF, Burnett EFP. Simplified Prediction of Driving Rain Deposition. In: Proc. of International Building Physics Conference, p. 375-382, Eindhoven: 2000.

[28] Blocken B, Carmeliet J. Overview of three state-of-the-art wind-driven rain assessment models and comparison based on model theory. Build Environ 2010; 45: 691–703. (doi:10.1016/j.buildenv.2009.08.007)

[29] Blocken B, Deszö G, van Beeck J, Carmeliet J. Comparison of calculation models for wind-driven rain deposition on building facades. Atmos Environ 2010;44: 1714–25. (doi:10.1016/j.atmosenv.2010.02.011)

[30] Blocken B, Abuku M, Nore K, Briggen PM, Schellen HL, Thue JV, et al. Intercomparison of wind-driven rain deposition models based on two case studies with full-scale measurements. J Wind Eng Ind Aerodyn 2011;99:448–59. (doi:10.1016/j.jweia.2010.11.004)

[31] Lacasse MA, O'Connor T, Nunes SC, Beaulieu P. Report from Task 6 of MEWS Project: Experimental assessment of water penetration and entry into wood-frame wall specimens – Final Report. (Internal Report 113). Institute for Research in Construction, National Research Council Canada, Ottawa: 2003.

[32] Mayo AP. To develop a European standard dynamic watertightness test for curtain walling. Task 3. Define the conditions to be reproduced in the standard test. Building Research Establishment (BRE), Watford: 1998.

[33] Balkema A, de Haan L. Residual life time at great age. Ann Probab 1974;2:792–04.

[34] Pickands J. Statistical inference using extreme order statistics. Ann Stat 1975;3(1):119–31.

[35] Smith RL. Threshold methods for sample extremes. In: Tiago J, editor. Statistical Extremes and Applications, NATO ASI Series Reidel. Dordrecht: 1985, p.623−38.

[36] Smith RL. Estimating tails of probability distributions. Ann Stat 1987;15:1174−207.

[37] Hoppestad S. Slagregn i Norge (*Driving rain in Norway, in Norwegian*). Norwegian Building Research Institute Report no. 13, Oslo: NBI; 1955.

[38] Lacy RE. Driving-rain maps and the onslaught of rain on buildings. Proceedings of RILEM/CIB symposium on moisture problems in buildings, Helsinki: 1965.

[39] Lacy RE. Climate and Building in Britain. Her Majesty's Stationery Office, London: 1977.

[40] Welsh RE, Skinner WR, Morris RJ. A climatology of driving rain pressure for Canada. Climate and Atmospheric Research Directorate Draft Report, Environment Canada, Atmospheric Environment Service; 1989.

[41] Choi ECC. Simulation of wind-driven rain around a building. J Wind Eng Ind Aerodyn 1993;46-47:721-9. (doi:10.1016/0167-6105(93)90342-L)

[42] Choi ECC. Parameters affecting the intensity of wind-driven rain on the front face of a building. J Wind Eng Ind Aerodyn 1994;53(1-2):1-17. (doi:10.1016/0167-6105(94)90015-9)

[43] Blocken B, Carmeliet J. Spatial and temporal distribution of driving rain on a low-rise building. Wind Struct 2002;5(5):441-62.

[44] Ray M, Rogers AL, McGowan JG. Analysis of wind shear models and trends in different terrains. In: Proceedings of the American Wind Energy Association Windpower 2005 Conference. Pittsburgh: 2006.

[45] WMO. Guide to Meteorological Instruments and Methods of Observation. WMO-No 8. World Meteorological Organization, Geneva: 2008.

[46] Cóstola D, Blocken B, Hensen JLM. Overview of pressure coefficient data in building energy simulation and airflow network programs. Build Environ 2009; 44(10): 2027-2036. (doi: 10.1016/j.buildenv.2009.02.006)

[47] Dingle AN, Lee Y. Terminal fall speeds of raindrops. Journal of Applied Meteorology 1972;11:877–9.

[48] Cornick SM, Dalgliesh A, Said N, Djebbar R, Tariku F, Kumaran MK. Report from Task 4 of MEWS Project: Task 4 – Environmental conditions final report (Research Report No. 113). National Research Council Canada. Ottawa: 2002.

[49] Bayes T. An essay towards solving a problem in the doctrine of chances. Philosophical Transactions of the Royal Society of London 1763;53:370–418. (doi:10.1098/rstl.1763.0053)

[50] Gumbel EJ. Statistics of extremes. Columbia University Press. New York: 1958.

[51] Lang M, Ouarda TBMJ, Bobée B. Towards operational guidelines for over-threshold modeling. Journal of Hydrology 1999;225:103–17.

[52] Pérez JM, Domínguez J, Rodríguez B, del Coz JJ, Cano E. Estimation of the exposure to moisture in Spain from daily wind and rain data. Build Environ 2012; 57: 259-70. (doi:10.1016/j.buildenv.2012.05.010)

[53] Pérez JM, Domínguez J, Rodríguez B, del Coz JJ, Cano E. Review and improvement of the water tightness degree required by the CTE DB-HS1 for building façades. Inf Constr 2013; Accepted article, In press.

[54] Pérez JM, Domínguez J, Rodríguez B, del Coz JJ, Cano E. Combined use of wind-driven rain and wind pressure to define water penetration risk into building façades: the Spanish case. Build Environ 2013;64:46-56. (doi:10.1016/j.buildenv.2013.03.004)

List of tables

Table 1. Intersection points and line equations associated with different return periods, obtained via POT analysis.

Table 2. Watertightness test parameters calculated by the Pareto-front method for different return periods and exposure combinations in the considered façade (z = 10 m, Bilbao).

Table 3. Summary of the highest annual precipitation recorded in a 10-minute interval and the calculation of Gumbel distribution parameters.

Table 4. Summary of the highest annual wind velocity recorded in a 10-minute interval and the calculation of the Gumbel distribution parameters.

Table 5. Watertightness test parameters calculated by the Bayesian performance-based method for different return periods and exposure combinations in the considered façade (z = 10 m, Bilbao). *The values fixed for solving the equation system are shown in bold type.*

Table 1.
Intersection points and line equations associated with different return periods, obtained by a POT analysis.

Return period	*Y-Intersection*	*Line equation in the scatterplot*
5	16.319	$R_h = -0.75897 \cdot U_{10} + 16.319$
10	17.624	$R_h = -0.75897 \cdot U_{10} + 17.624$
15	18.394	$R_h = -0.75897 \cdot U_{10} + 18.394$
20	18.944	$R_h = -0.75897 \cdot U_{10} + 18.944$
25	19.371	$R_h = -0.75897 \cdot U_{10} + 19.371$
30	19.722	$R_h = -0.75897 \cdot U_{10} + 19.722$
40	20.278	$R_h = -0.75897 \cdot U_{10} + 20.278$
50	20.711	$R_h = -0.75897 \cdot U_{10} + 20.711$
75	21.501	$R_h = -0.75897 \cdot U_{10} + 21.501$
100	22.065	$R_h = -0.75897 \cdot U_{10} + 22.065$

Table 2.
Watertightness test parameters calculated by the Pareto-front method for different return periods and exposure combinations in the considered façade (z = 10 m, Bilbao).

Return period	*Extreme R_h combination*				*Extreme U_{10} combination*				*Moderate U_{10} and R_h combination*			
	R_h	U_{10}	WDR	DRWP	R_h	U_{10}	WDR	DRWP	R_h	U_{10}	WDR	DRWP
5	21.68	7.06	2.072	29.900	0.96	20.24	0.449	245.740	5.89	13.75	1.342	113.405
10	23.97	8.37	2.678	42.004	1.31	21.49	0.613	277.195	6.22	15.03	1.536	135.534
15	25.33	9.14	3.067	50.111	1.52	22.24	0.714	296.648	6.41	15.79	1.655	149.519
20	26.30	9.69	3.359	56.332	1.67	22.76	0.789	310.931	6.55	16.33	1.743	159.917
25	27.05	10.12	3.595	61.429	1.78	23.18	0.848	322.288	6.66	16.75	1.812	168.258
30	27.67	10.47	3.793	65.773	1.88	23.51	0.897	331.750	6.75	17.09	1.870	175.253
40	28.65	11.03	4.117	72.955	2.03	24.05	0.976	347.016	6.89	17.64	1.963	186.624
50	29.41	11.46	4.377	78.808	2.14	24.47	1.040	359.145	7.00	18.06	2.038	195.729
75	30.80	12.25	4.871	90.078	2.35	25.23	1.158	381.833	7.20	18.84	2.176	212.916
100	31.79	12.82	5.238	98.580	2.51	25.77	1.245	398.445	7.35	19.39	2.277	225.621

Return period (years); R_h (l/m^2 10 min); U_{10} (m/s); WDR (l/m^2 min); DRWP (Pa)

Table 3.
Summary of the highest annual precipitation recorded in a 10-minute interval and the calculation of Gumbel distribution parameters.

Bilbao airport. Station 1082. 43º17'53"N 02º54'21"W			
Year	Máximum R_h (l/m^2 in 10 minutes)	Year	Máximum R_h (l/m^2 in 10 minutes)
1997	10.1	2004	6.5
1998	9.1	2005	12.7
1999	6.3	2006	10.7
2000	9.0	2007	10.2
2001	9.9	2008	8.9
2002	6.7	2009	10.2
2003	6.9	2010	6.7

Magnitude	Value	Comment
N	14	Number of x_i data.
$\bar{x}$	8.85000	Data average: $\bar{x} = \sum x_i / N$
σ_x	1.88443	Standard deviation: $\sigma_x = \sqrt{\sum (x_i - \bar{x})^2 / N}$
λ_y	0.51000	Data average of 1 to N y_i values (reduced variable): $y_i = -\ln(\ln(^{N+1}/_{i}))$ *(Only depends on N value and could be approximated by a constant value of 0,5772)*
σ_y	1.00950	Standard deviation of 1 to N y_i values (reduced variable): $y_i = -\ln(\ln(^{N+1}/_{i}))$ *(Only depends on N value and could be approximated by a constant value of 1,2856)*
$\lambda_{(Rh)}$	**7.89788**	Mode: $\lambda = \bar{x} - \lambda_y \frac{\sigma_x}{\sigma_y}$
$\beta_{(Rh)}$	**1.86674**	Dispersion parameter: $\beta = \frac{\sigma_x}{\sigma_y}$

Table 4.
Summary of the highest annual wind velocity recorded in a 10-minute interval and the calculation of Gumbel distribution parameters.

Bilbao airport. Station 1082. 43º17'53"N 02º54'21"W			
Year	Máximum U_{10} (m/s)	Year	Máximum U_{10} (m/s)
1997	15.0	2004	17.7
1998	13.0	2005	16.7
1999	17.6	2006	18.2
2000	12.4	2007	19.1
2001	12.7	2008	18.6
2002	13.6	2009	20.9
2003	16.8	2010	15.4

Magnitude	Value	Comment
N	14	Number of x_i data.
$\bar{x}$	16.26429	Data average: $\bar{x} = \sum x_i / N$
σ_x	2.54660	Standard deviation: $\sigma_x = \sqrt{\sum (x_i - \bar{x})^2 / N}$
λ_y	0.51000	Data average of 1 to N y_i values (reduced variable): $y_i = -\ln(\ln(^{N+1}/_{i}))$ *(Only depends on N value and could be approximated by a constant value of 0,5772)*
σ_y	1.00950	Standard deviation of 1 to N y_i values (reduced variable): $y_i = -\ln(\ln(^{N+1}/_{i}))$ *(Only depends on N value and could be approximated by a constant value of 1,2856)*
$\lambda_{(U10)}$	**14.97760**	Mode: $\lambda = \bar{x} - \lambda_y \frac{\sigma_x}{\sigma_y}$
$\beta_{(U10)}$	**2.52269**	Dispersion parameter: $\beta = \frac{\sigma_x}{\sigma_y}$

Table 5.
Watertightness test parameters calculated by the Bayesian performance-based method for different return periods and exposure combinations in the considered façade (z = 10 m, Bilbao). *The values fixed for solving the equation system are shown in bold type*.

Return period	*Extreme R_h combination*				*Extreme U_{10} combination*				*Moderate U_{10} and R_h combination*			
	R_h	U_{10}	WDR	DRWP	R_h	U_{10}	WDR	DRWP	R_h	U_{10}	WDR	DRWP
5	10.40	13.18	**2.072**	104.230	1.06	18.75	**0.449**	210.979	5.52	14.51	**1.342**	126.339
10	-	-	**2.678**	-	1.38	20.64	**0.613**	255.684	5.85	15.82	**1.536**	150.094
15	-	-	**3.067**	-	1.56	21.72	**0.714**	282.972	6.05	16.56	**1.655**	164.620
20	-	-	**3.359**	-	1.69	22.47	**0.789**	302.934	6.20	17.09	**1.743**	175.263
25	-	-	**3.595**	-	1.79	23.04	**0.848**	318.569	6.32	17.50	**1.812**	183.758
30	-	-	**3.793**	-	1.88	23.51	**0.897**	331.652	6.42	17.83	**1.870**	190.796
40	-	-	**4.117**	-	2.01	24.25	**0.976**	352.735	6.57	18.36	**1.963**	202.161
50	-	-	**4.377**	-	2.11	24.81	**1.040**	369.411	6.69	18.76	**2.038**	211.177
75	-	-	**4.871**	-	2.29	25.85	**1.158**	400.965	6.91	19.50	**2.176**	228.048
100	-	-	**5.238**	-	2.41	26.58	**1.245**	423.920	7.07	20.02	**2.277**	240.404

Return period (years); R_h (l/m^2 10 min); U_{10} (m/s); WDR (l/m^2 min); DRWP (Pa)

Figure captions

Fig. 1. Overall scheme of Pareto-front method and its graphic procedure.

Fig. 2. Overall scheme of Bayesian performance-based method and its equation system solution.

Fig. 3. Scatterplot showing 15 years of 10-minute rainfall intensities and simultaneous wind velocities (*grey dots represent Pareto-points not contained in the first 10 Pareto-fronts*).

Fig. 4. Empirical CDF of intersection values (grey line) and theoretical CDF of a GPD with γ = 0.0161647, σ = 1.77267 and optimal threshold u = 10.1895 (black line).

Fig. 5. The line intersections represent the interesting climate variables for different exposure combinations and return periods (*maximum R_h or U_{10} Pareto-point of each Pareto-front are also shown*).

Fig. 6. Graphic solution of the Eqs. 2 and 4' system for the extreme R_h combination (Table 2): 5-year return period (black lines) and 10-year return period (grey lines).

Fig. 7. Estimated ΔP values calculated by both methods to simulate extreme U_{10} combinations for the same WDR values and return periods in the considered façade (z = 10 m, Bilbao).

Fig. 8. Estimated ΔP values calculated by both methods to simulate moderate U_{10}-R_h combinations for the same WDR values and return periods in the considered façade (z = 10 m, Bilbao).

Figure 1

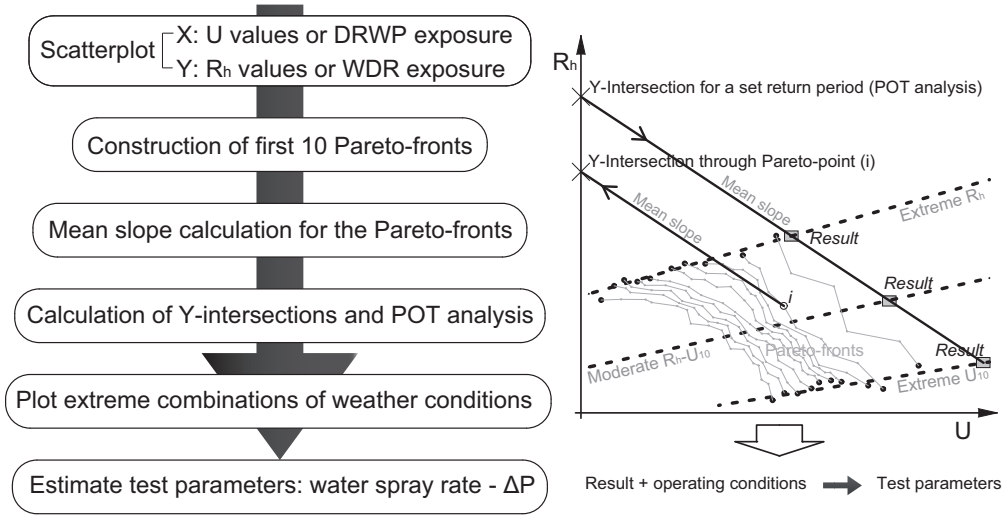

Fig. 1. Overall scheme of Pareto-front method and its graphic procedure.

Figure 2

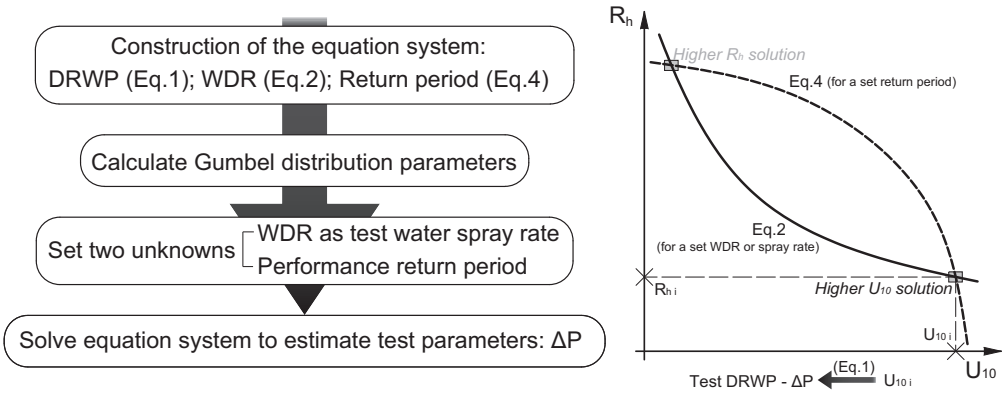

Fig. 2. Overall scheme of Bayesian performance-based method and its equation system solution.

Figure 3

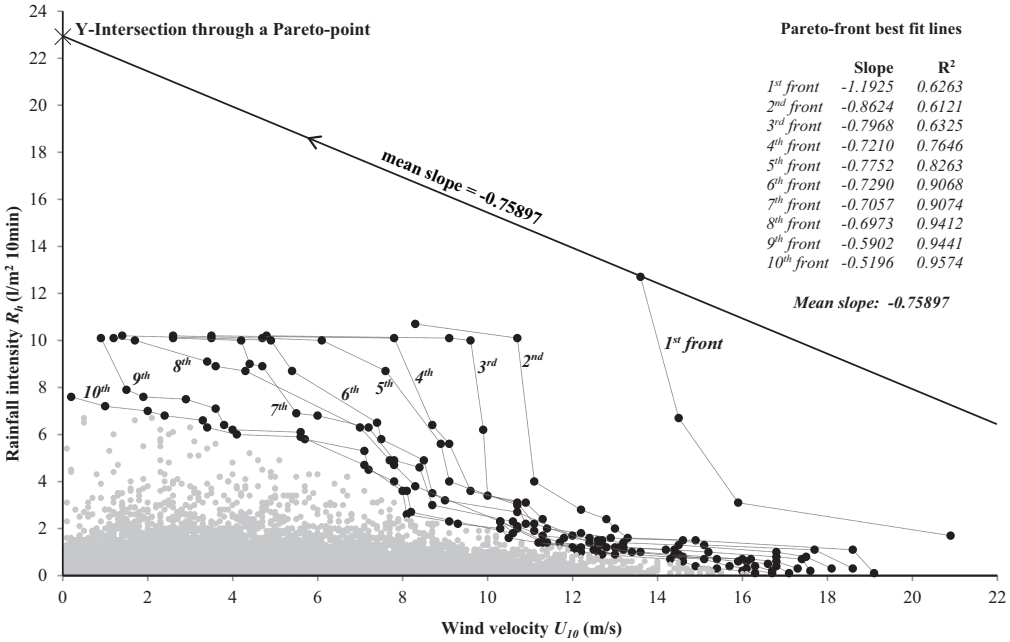

Fig. 3. Scatterplot showing 15 years of 10-minute rainfall intensities and simultaneous wind velocities *(grey dots represent Pareto-points not contained in the first 10 Pareto-fronts).*

Figure 4

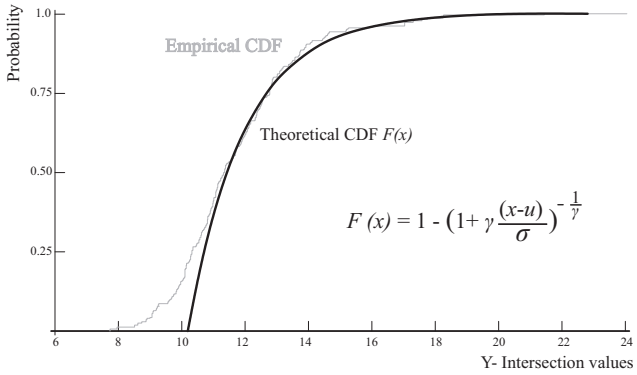

Fig. 4. Empirical CDF of intersection values (grey line) and theoretical CDF of a GPD with γ =0.0161647, σ =1.77267 and optimal threshold u =10.1895 (black line).

Figure 5

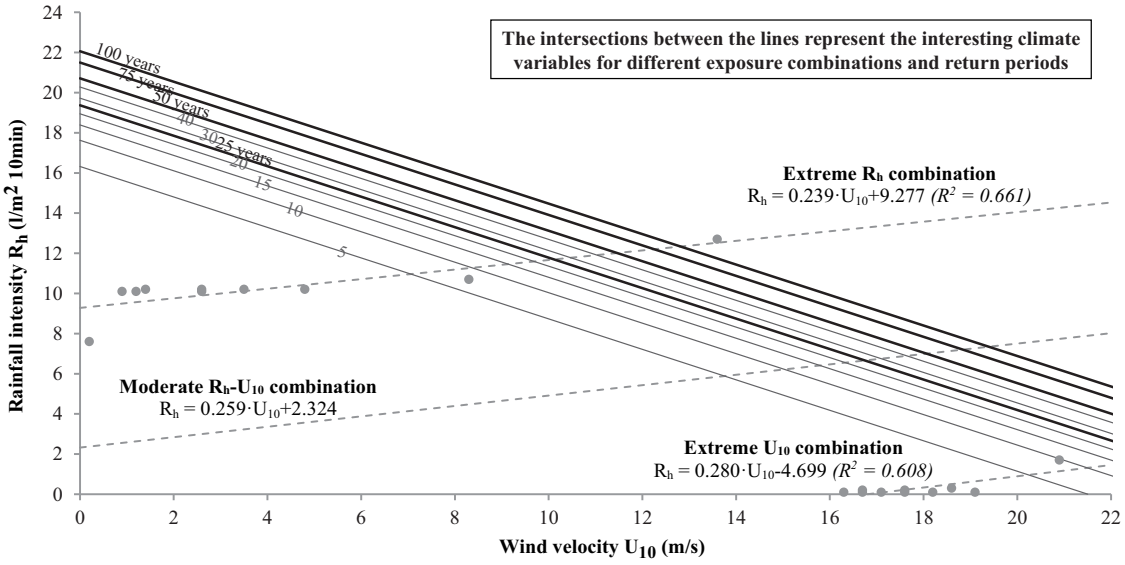

Fig. 5. The line intersection represent the interesting climate variables for different exposure combinations and return periods *(maximum R_h or U_{10} Pareto-point of each Pareto-front are also shown).*

Figure 6

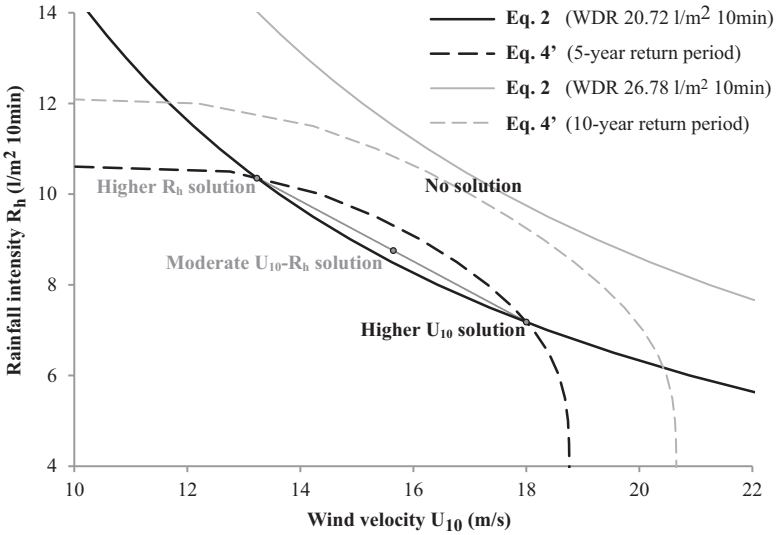

Fig. 6. Graphic solution of the Eqs. 2 and 4' system for the extreme R_h combination (Table 2): 5-year return period (black lines) and 10-year return period (grey lines).

Figure 7

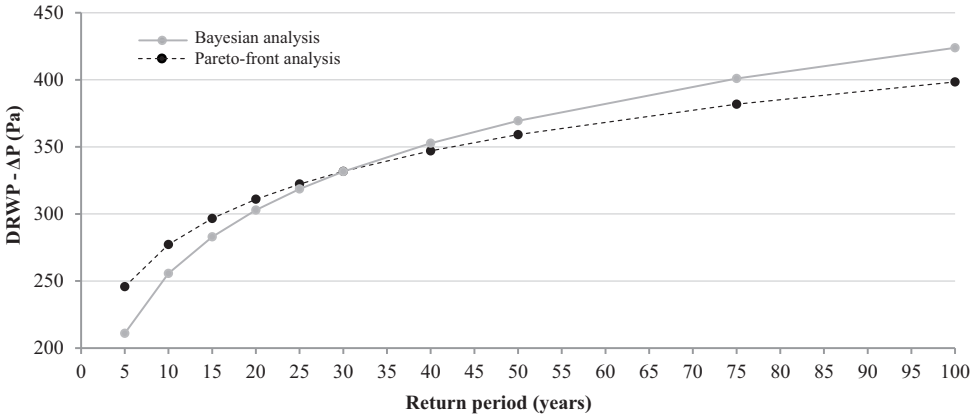

Fig. 7. Estimated ΔP values calculated by both methods to simulate extreme U_{10} combinations for the same WDR values and return periods in the considered façade (z = 10 m, Bilbao).

Figure 8

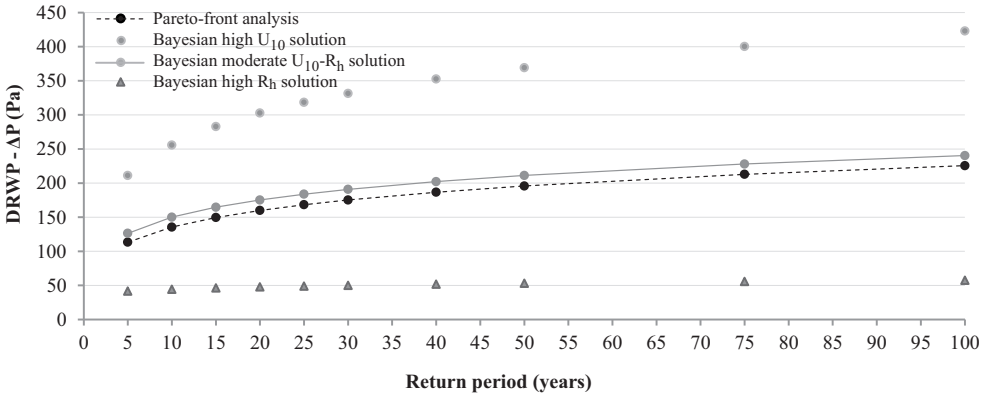

Fig. 8. Estimated ΔP values calculated by both methods to simulate moderate U_{10}-R_h combinations for the same WDR values and return periods in the considered façade (z = 10 m, Bilbao).